Materials Today Communications 26 (2021) 101920

Contents lists available at ScienceDirect

Materials Today Communications

journal homepage: www.elsevier.com/locate/mtcomm

Quantitative analysis of grain structure and texture evolution of dissimilar AA2024/7075 joints manufactured by friction stir welding

Chenghang Zhang [a,b], Guangjie Huang [a,b,*], Qing Liu [c]

[a] International Joint Laboratory for Light Alloys (MOE), College of Materials Science and Engineering, Chongqing University, Chongqing, 400044, PR China
[b] Shenyang National Laboratory for Materials Science, Chongqing University, Chongqing, 400044, PR China
[c] College of Materials Science and Engineering, Nanjing Tech University, Nanjing, 211816, PR China

ARTICLE INFO

Keywords:
Friction stir welding
Aluminum alloys
Welding speed
Grain structure
Recrystallization
Shear texture

ABSTRACT

Friction stir welding (FSW) can successfully join aluminum alloys that are difficult to weld. However, FSW causes texture inhomogeneity in the nugget zone (NZ), which may affect the integrality of joints. Thus, a quantitative study on the grain structure and texture evolution of the NZ in dissimilar AA2024 and AA7075 joints at three welding speeds was performed via electron backscatter diffraction. The results showed that dynamic recrystallization in the NZ generates fine equiaxed grains instead of elongated grain microstructure in base materials. The average grain size and recrystallization degree are reduced with the increment in welding speed. Different kinds of shear texture components are formed and the shear textures are significantly decreased from 66.4% to 12.1% with the decrease in welding speed from 240 mm/min to 60 mm/min. The variation in grain structure and shear textures depends largely upon the welding heat inputs at different welding speeds. The research contributes to understanding the mechanism of microstructure homogenization in FSW joints and further optimizing welding process for engineering application.

1. Introduction

For high strength 2xxx and 7xxx aluminum alloys that are hard to weld, friction stir welding (FSW) is regarded as an ideal welding technology to optimize the local microstructures of the joints, thus imparting good mechanical properties [1–4]. However, the intricate thermo-mechanical inputs induced during FSW lead to heterogeneity of the joints. This inhomogeneous microstructure distribution, including the grain structure and texture in the joint that are affected by the FSW tool, has a conspicuous influence on joint integrity and subsequent mechanical performance [5].

Some researchers have reported microstructural and crystallographic texture evolution on similar FSW aluminum alloys joints. For example, Wang et al. [6] concluded that using different rotational speeds results in the generation of different shear texture components in the stir zone of FSW AA6061-T6 joints. Similarly, Shen et al. [7] found that upper and lower joint zones experienced various shear distortions, results in different shear texture types. Moreover, Imam et al. [8] reported that different types of textures are generated at the top and bottom areas in FSW AA6063 joints, and also found a periodic variation in the onion ring area. Liu et al. [9] found that preferential grain growth occurs along $\{112\}\langle 110\rangle$ in FSW AA1050-H2 joints. Chen et al. [10] performed FSW of AA2A97 Al-Li alloys and found that the initial textures of copper and brass components of the base materials (BMs) are weakened in the joints while the recrystallization texture intensity is stronger at high rotational speeds.

Because FSW is asymmetric, different zones in dissimilar joints undergo various plastic deformations and heat inputs, which leads to more inhomogeneous microstructure than in similar joints. Thus it is essential to perform microstructure and textures evolution in dissimilar FSW joints. Moradi et al. [11] investigated dissimilar FSW AA2024/6061 joints and found that the original textures disappeared and some shear components with high intensity were formed in the joints. Wang et al. [12] conducted FSW of dissimilar AA5052-O/6061-T6 joints and concluded that the $\{111\}\left\langle \bar{1}1\bar{2}\right\rangle A_1^*$ components is formed in the nugget zone (NZ). However, there are few studies on the quantitative analysis of grain microstructure and texture components in dissimilar FSW AA2024/7075 joints.

Although studies have been conducted on texture analysis in

* Corresponding author at: International Joint Laboratory for Light Alloys (MOE), College of Materials Science and Engineering, Chongqing University, Chongqing, 400044, PR China.
E-mail address: gjhuang@cqu.edu.cn (G. Huang).

https://doi.org/10.1016/j.mtcomm.2020.101920
Received 14 July 2020; Received in revised form 7 August 2020; Accepted 24 November 2020
Available online 30 November 2020

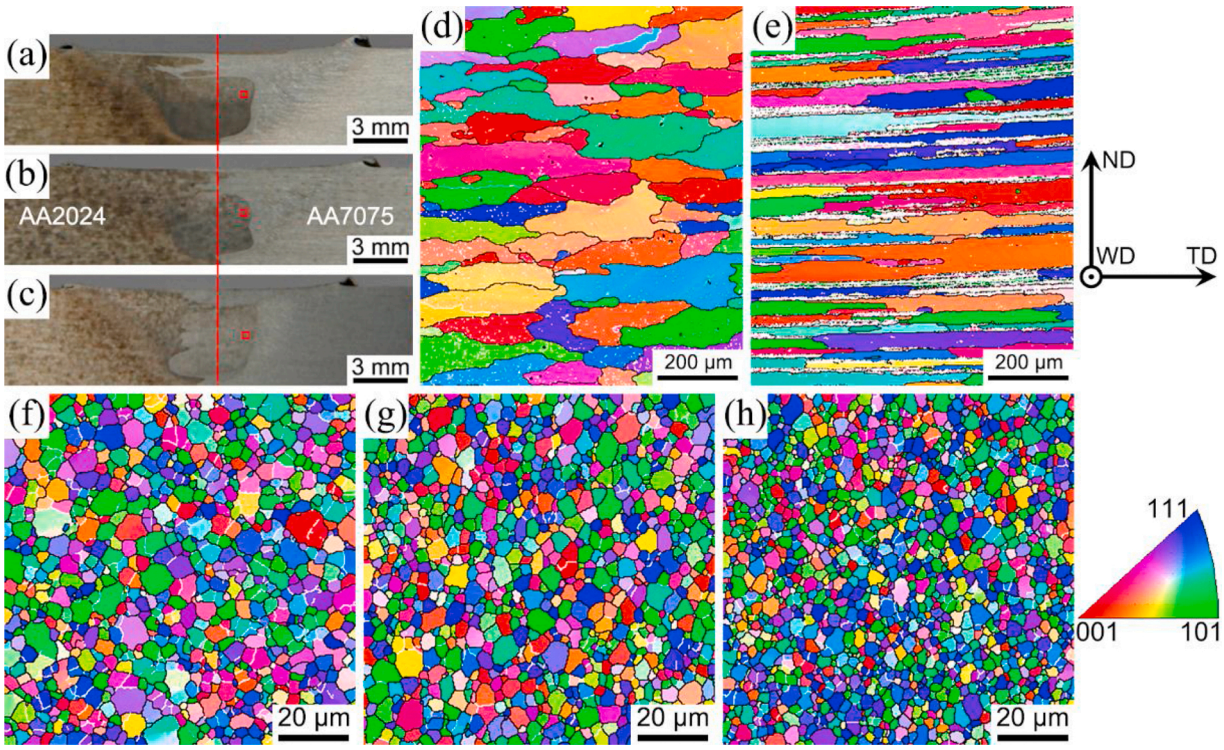

Fig. 1. Transverse morphologies of the samples: (a) 60 mm/min, (b) 100 mm/min and (c) 240 mm/min, EBSD orientation maps (d) AA2024, (e) AA7075, (f) 60 mm/min, (g) 100 mm/min and (h) 240 mm/min.

dissimilar welds and identification of texture types of different local zones in the joints at various FSW welding parameters [13–17], a quantitative analysis of grain microstructure and shear texture components in dissimilar AA2024/7075 welds is lacking. In the present study, we conducted grain microstructure and texture analysis in the NZ of dissimilar AA2024/7075 welds by using electron back-scattering diffraction (EBSD).

2. Experimental procedure

6.5 mm thick AA2024-T351 and AA7075-T651 plates—300 mm long and 40 mm wide—were selected for the friction stir butt welding experiment which was executed at a fixed rotational speed of 1300 rpm and three welding speeds (60, 100, and 240 mm/min) along the transverse direction (TD; normal to the rolling direction, RD) of the two BMs. The placement of the two BMs was as follows: AA2024-T351 in the advancing side (AS) and AA7075-T651 in the retreating side (RS). Prior to welding, the surface of the BMs was sanded bright. The shoulder diameter of the FSW tool was 15 mm while the tool pin height and pin tip diameter with a tapered thread were 5 mm and 3.76 mm, respectively. Microstructural analysis was carried out on the joint cross section, which was normal to the welding direction (WD), using the EBSD technique. EBSD analysis was executed using a field emission scanning electron microscopy (FESEM, TESCAN MIRA3) equipped with an HKL-EBSD system, which was operated at 20 kV. The step size was set at 0.3 μm, and all the EBSD data were disposed via Channel 5 software. The measured specimens—20 mm long and 6 mm wide—including the entire welded regions, were cut from the joint cross section, prepared by a standard metallographic procedure, and finally electropolished by a mixed solution comprising perchloric acid and alcohol (1:9, volume ratio) at 2–5 °C at 15 V for 100 s.

3. Results and discussion

The cross-sectional features of the joints are shown in Fig. 1a. Due to the fact that AA2024 BM is more sensitive to etchant than A7075 BM, the dark area on the left is AA2024 BM while the light area on the right is AA7075 BM. During FSW, the plasticized metals produced by friction

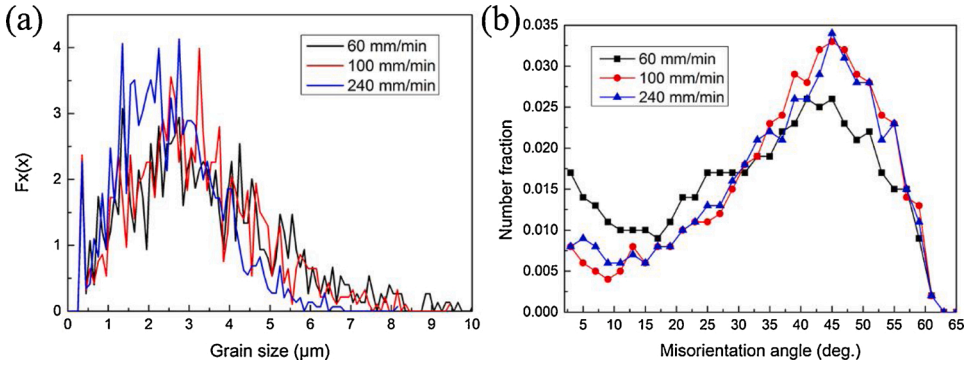

Fig. 2. The grain size distribution (a) and the distribution of misorientation angle (b) of the NZ in three joints.

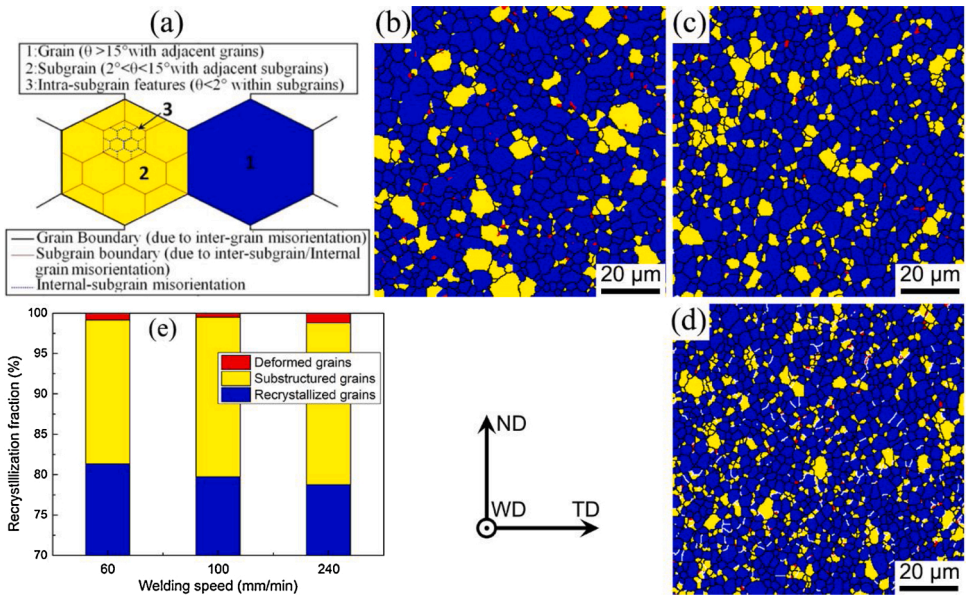

Fig. 3. (a) The features of different kinds of grains [19], (b) 60 mm/min, (c) 100 mm/min, (d) 240 mm/min and (e) the statistic results of the different kinds of grains.

and agitation of the tool are moved from the front to the rear of the tool to fill the cavity behind the tool, finally forming a dense solid phase joining the two BMs. The complicated material flow response takes place in the NZ through the stirring of the tool. It can be clearly observed that AA2024 on the AS flows to AA7075 on the RS while AA 2024 occupies the majority of the NZ. According to our previous work [14], the microstructure near the interface area where the two BMs are mixed is relatively complex; thus, we analyze this area in this work as illustrated in the red rectangle in Fig. 1a.

The orientation distribution maps of the specimens are displayed in Fig. 1d-h. The grains of the two BMs are typical lamellar and elongated along the RD (Fig. 1d and e), {001}<100> Cube component presents in AA2024-T351 BM and the two texture components, ({011}<211> Brass, and {123}<634 > S, are mainly developed in AA7075-T651,

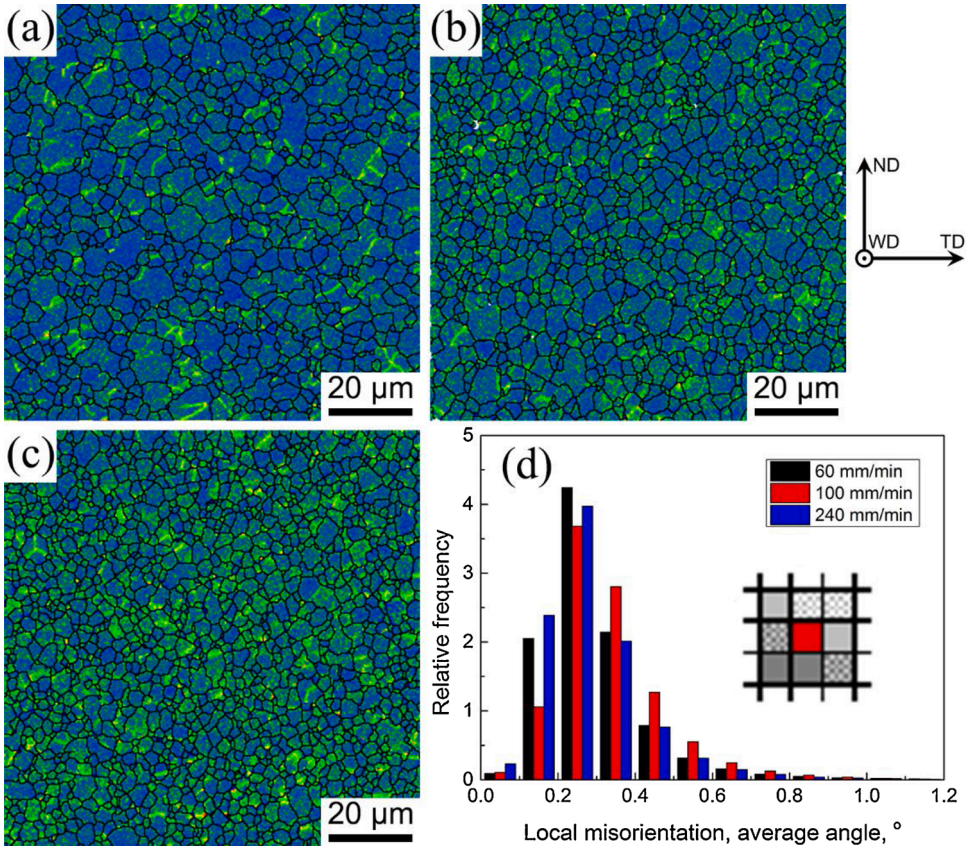

Fig. 4. Local misorientation distribution maps (a) 60 mm/min, (b) 100 mm/min, (c) 240 mm/min and (d) the statistics results of local misorientation distribution.

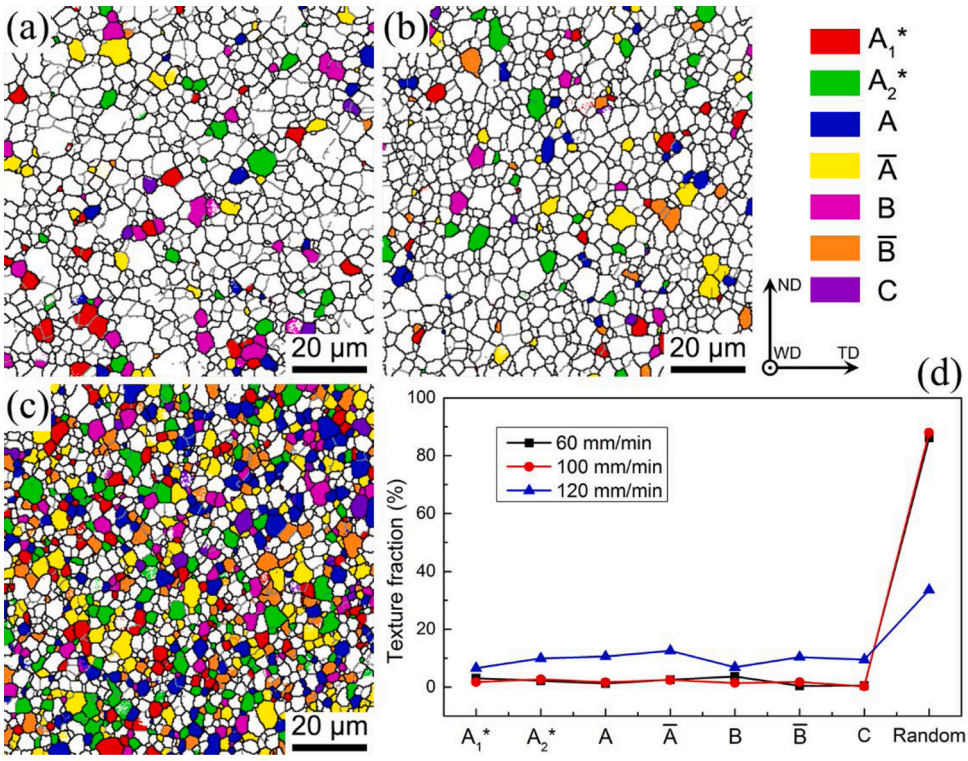

Fig. 5. Distribution of different shear texture types in the joints: (a) 60 mm/min, (b) 100 mm/min, (c) 240 mm/min and (d) the statistic results of textures.

according to our previous research [14]. In the NZ, bulk fine equiaxed grains (Fig. 1f-h) are produced because dynamic recrystallization (DRZ) occurs in the NZ owing to the significant shear distortion and high thermal cycle caused by the tool. Fig. 2a shows the grain size distribution of the NZ in the three joints; the calculated average grain size in the joints at 60, 100, and 240 mm/min is 3.34 ± 1.8 μm, 3.15 ± 1.6 μm, and 2.54 ± 1.2 μm, respectively. It can be seen that the average grain size decreases with an increase in welding speed. During FSW, the produced the heat input can be evaluated as follows [18]:

$$Q = \frac{4\pi^2 \mu P \omega R^3}{3V} \quad (1)$$

where Q, μ, P, R, ω and V are heat input rate per unit weld length, friction coefficient, pressure, shoulder radius, rotational speed and welding speed, respectively. Thus, it is concluded that high heat input is produced at low welding speeds, resulting in grain growth in the NZ. Fig. 2b shows the distribution of the misorientation angle in the three joints. High angle grain boundaries (HAGBs) of more than 15° are marked with a black line while low angle grain boundaries (LAGBs) from 2°-15° is marked with white lines in Fig. 1f-h. From the statistic results in Fig. 2b, we see that by increasing the welding speed from 60 to 100 and 240 mm/min, the percentage of LAGBs are 8.6 %, 10.3 %, and 17.5 %, respectively, while the percentage of HAGBs are respectively 91.4 %, 89.7 %, and 82.5 %, respectively.

Fig. 3a shows the features of grains, substructured grains and inter substructured grains. The distribution of the calculated deformed, substructured and recrystallized grains are illustrated in Fig. 3b-d while their statistic results are summarized in Fig. 3e. The percentage of substructured and recrystallized grains in the NZ of the joint at 60 mm/min were 17.8 % and 81.3 %, respectively. With the increase in welding speed, the fraction of the substructured grains of the joint increased while that of the recrystallized grains decreased. As the welding speed increased to 240 mm/min, the maximum fraction of the substructured grains in the joint was 20.1 % while the minimum fraction of the recrystallized grains was 78.8 %. It is concluded that the degree of recrystallization is increased at low welding. This is largely associated with the heat input during FSW. A low welding speed can produce a high heat input which leads to a high degree of recrystallization by consuming more substructured grains.

Rotation, friction, extrusion, and movement of the tool result in the dislocation being consumed in motion which makes the material more prone to deformation. During microstructure evolution, heat generation and mechanical deformation influence dislocation regeneration, rearrangement, or re-consumption. Thus, we can evaluate the microstructure evolution based on dislocation variation. Fig. 4 shows distribution maps of the local misorientation angle which represents the average misorientation value between each pixel and its eight neighbors; this is in accordance with the amounts of the LAGBs (Fig. 2b) and substructured grains (Fig. 3). Dislocation density is expressed using the local misorientation θ_{loc} [20]:

$$\rho = \frac{\alpha \theta_{loc}}{ndb} \quad (2)$$

in which α and n are grain boundary parameters and defined area size, respectively, while d and b are the step size of EBSD tests and the Burgers vector, respectively. It is concluded that a high level of local misorientation values means a high level of accumulated dislocations. Thus, the local misorientation distribution maps in Fig. 4 reveal that the dislocation density of the NZ is reduced with decreasing welding speed. The low fraction of the substructured grains in the NZ of the joint at 60 mm/min results from the overlay of the quasi-static load on local residual softening. Stress overlay can induce dislocation regeneration, rearrangement or re-consumption to produce potent dislocation position for the formation of the substructured grains [19]. A lower welding speed produces more heat input and causes grain growth by consuming more dislocation within grains which gives rise to an increase in the fraction of recrystallized grains [21]. Accordingly, high heat input can promote the degree of recrystallization to some extent.

The rotation and extrusion of the tool result in the occurrence of violent shear deformation and high peak temperature which form the shear textures. During deformation, the {111} slip plane is aligned to the

shear plane while the <110> slip direction is aligned to the shear direction. For FCC metals, there are {111}<uvw > A fiber and {hkl}< 110 > B fiber; their specific types are [22]: $\{111\}<\overline{1}\overline{1}2>A_1^*$ 、 $\{111\}<11\overline{2}>A_2^*$ 、 $\left\{1\overline{1}1\right\}<110>A$ 、 $\left\{\overline{1}1\overline{1}\right\}<\overline{1}\overline{1}0>\overline{A}$ 、 $\left\{1\overline{1}2\right\}<110>B$ 、 $\left\{\overline{1}1\overline{2}\right\}<\overline{1}\overline{1}0>\overline{B}$ and $\{001\}<110>C$. The shear texture types generated in the NZ at different welding speeds were analyzed using channel 5 software as shown in Fig. 5a-c, which demonstrate the distribution of different shear texture types using different colors. Fig. 5d shows quantitative statistic results of the shear texture content in the NZ at different welding speeds. It was observed that the total amount of shear texture in the NZ increased from 12.1% to 66.4% with increasing welding speed—from 60 mm/min to 240 mm/min, respectively. Obviously, a higher welding speed (240 mm/min) produces higher total shear textures. Compared to the other shear textures, A_1^* and A_2^* components, 5.32 % and 4.47 %, respectively, are predominant at 60 and 100 mm/min while A and $\overline{A}$ are the main components at a high welding speed (240 mm/min), which is approximately 23.2 % in total. Furthermore, the distributions of different types of shear texture components are more dispersive in the joint at higher welding speeds, as indicated in Fig. 5c. Compared to a low welding speed, a high welding speed produces low heat input, and the fine grains formed in the NZ have no time to grow; therefore, the resulting shear textures are preserved. In contrast, a low welding speed produces high heat input, consumes a certain amount of fine grains, and then grow to a certain extent, resulting in the disappearance of the newly generated shear texture. Thus the total content of shear textures is low compared to that at low welding speeds. On the other hand, random texture content shows the opposite trend.

4. Conclusions

DRZ occurs in the NZ, forming fine equiaxed grains. With a decrease of welding speed from 240 mm/min to 60 mm/min, the average grain size increased from 2.54 ± 1.2 μm to 3.34 ± 1.8 μm. Similarly, the fraction of recrystallized grains increased from 78.8 % to 81.3 % while the fraction of LAGBs decreased from 17.5 % to 8.6 %. This is because a low welding speed produces a high thermal cycle in the NZ, which facilities grain growth and recrystallization. Different types of shear texture are generated in the NZ. The total amount of shear texture in the NZ decreased from 66.4 % to 12.1 % when the welding speed decreased from 240 mm/min to 60 mm/min because a low welding speed produces high heat input, giving rise to a high degree of recrystallization and grain growth.

Declaration of Competing Interest

We declare that we do not have any commercial or associative interest that represents a conflict of interest in connection with the work submitted.

Acknowledgements

The “National Natural Science Foundation of China” (NO. 51421001) and “Fundamental Research Funds for the Central Universities” (No. 2018CDJDCL0019) are greatly acknowledged for financial support. The Electron Microscopy Center of Chongqing University is also greatly acknowledged for offering measurements.

References

[1] R.S. Mishra, Z. Ma, Friction stir welding and processing, Mat. Sci. Eng. R 50 (2005) 1–78.
[2] X. Meng, Y. Huang, J. Cao, J. Shen, J.F. dos Santos, Recent progress on control strategies for inherent issues in friction stir welding, Prog. Mater. Sci. (2020), 100706.
[3] C. Zhang, G. Huang, Y. Cao, Y. Zhu, W. Li, X. Wang, et al., Microstructure and mechanical properties of dissimilar friction stir welded AA2024-7075 joints: influence of joining material direction, Mater. Sci. Eng. A 766 (2019), 138368.
[4] C. Zhang, G. Huang, Y. Cao, Q. Li, Y. Zhu, X. Huang, et al., Investigation on microstructure and localized corrosion behavior in the stir zone of dissimilar friction-stir-welded AA2024/7075 joint, J. Mater. Sci. (2020) 1–28.
[5] W. Xu, Y. Luo, M. Fu, Microstructure evolution in the conventional single side and bobbin tool friction stir welding of thick rolled 7085-T7452 aluminum alloy, Mater. Charact. 138 (2018) 48–55.
[6] T. Wang, Y. Zou, K. Matsuda, Micro-structure and micro-textural studies of friction stir welded AA6061-T6 subjected to different rotation speeds, Mater. Des. 90 (2016) 13–21.
[7] J. Shen, F. Wang, U.F. Suhuddin, S. Hu, W. Li, J.F. Dos Santos, Crystallographic texture in bobbin tool friction-stir-welded aluminum, Metall. Mater. Trans. A 46 (2015) 2809–2813.
[8] M. Imam, V. Racherla, K. Biswas, H. Fujii, V. Chintapenta, Y. Sun, et al., Microstructure-property relation and evolution in friction stir welding of naturally aged 6063 aluminium alloy, Int. J. Adv. Manuf. Tech. 91 (2017) 1753–1769.
[9] X. Liu, Y. Sun, H. Fujii, Clarification of microstructure evolution of aluminum during friction stir welding using liquid CO2 rapid cooling, Mater. Des. 129 (2017) 151–163.
[10] H. Chen, L. Fu, P. Liang, Microstructure, texture and mechanical properties of friction stir welded butt joints of 2A97 AlLi alloy ultra-thin sheets, J. Alloys Compd. 692 (2017) 155–169.
[11] M.M. Moradi, H.J. Aval, R. Jamaati, S. Amirkhanlou, S. Ji, Microstructure and texture evolution of friction stir welded dissimilar aluminum alloys: AA2024 and AA6061, J. Manuf. Process. 32 (2018) 1–10.
[12] B. Wang, B.-b. Lei, J.-x. Zhu, Q. Feng, L. Wang, D. Wu, EBSD study on microstructure and texture of friction stir welded AA5052-O and AA6061-T6 dissimilar joint, Mater. Des. 87 (2015) 593–599.
[13] C. Zhang, G. Huang, Y. Cao, Y. Zhu, Q. Liu, On the microstructure and mechanical properties of similar and dissimilar AA7075 and AA2024 friction stir welding joints: effect of rotational speed, J. Manuf. Process. 37 (2019) 470–487.
[14] C. Zhang, Y. Cao, G. Huang, Q. Zeng, Y. Zhu, X. Huang, et al., Influence of tool rotational speed on local microstructure, mechanical and corrosion behavior of dissimilar AA2024/7075 joints fabricated by friction stir welding, J. Manuf. Process. 49 (2020) 214–226.
[15] Z. Chenghang, H. Guangjie, C. Yu, L. Wei, L. Qing, EBSD analysis of nugget zone in dissimilar friction stir welded AA2024-AA7075 joint along weld thickness, Rare Metal Mat. Eng. 48 (2019) 3161–3166.
[16] C. Zhang, G. Huang, Y. Cao, Q. Li, L. Niu, Q. Liu, Characterizations of microstructure, crystallographic texture and mechanical properties of dissimilar friction stir welding joints for AA2024 and AA7075 under different tool shoulder end profiles, Mater. Today Commun. (2020), 101435.
[17] C. Zhang, G. Huang, Y. Cao, Y. Zhu, X. Huang, Y. Zhou, et al., Microstructure evolution of thermo-mechanically affected zone in dissimilar AA2024/7075 joint produced by friction stir welding, Vacuum (2020), 109515.
[18] C. Yu, D. Hua, J.-z. Li, J.-w. Zhao, M.-j. Fu, X.-h. Li, Effect of welding heat input and post-welded heat treatment on hardness of stir zone for friction stir-welded 2024-T3 aluminum alloy, T. Nonferr. Metal. Soc. 25 (2015) 2524–2532.
[19] G. Padhy, C. Wu, S. Gao, Subgrain formation in ultrasonic enhanced friction stir welding of aluminium alloy, Mater. Lett. 183 (2016) 34–39.
[20] M. Calcagnotto, D. Ponge, E. Demir, D. Raabe, Orientation gradients and geometrically necessary dislocations in ultrafine grained dual-phase steels studied by 2D and 3D EBSD, Mater. Sci. Eng. A 527 (2010) 2738–2746.
[21] C. He, Y. Li, Z. Zhang, J. Wei, X. Zhao, Investigation on microstructural evolution and property variation along building direction in friction stir additive manufactured Al–Zn–Mg alloy, Mater. Sci. Eng. A 777 (2020), 139035.
[22] R. Fonda, J. Bingert, Texture variations in an aluminum friction stir weld, Scr. Mater. 57 (2007) 1052–1055.